crystals

MDPI

Article

X-ray Single Crystal Structure, Tautomerism Aspect, DFT, NBO, and Hirshfeld Surface Analysis of a New Schiff Bases Based on 4-Amino-5-Indol-2-yl-1,2,4-Triazole-3-Thione Hybrid

Ahmed T. A. Boraei [1,*], Saied M. Soliman [2], Matti Haukka [3], El Sayed H. El Tamany [1], Abdullah Mohammed Al-Majid [4] and Assem Barakat [4,*]

[1] Chemistry Department, Faculty of Science, Suez Canal University, Ismailia 41522, Egypt; s.eltamany51@yahoo.com
[2] Department of Chemistry, Faculty of Science, Alexandria University, P.O. Box 426, Ibrahimia, Alexandria 21321, Egypt; saied1soliman@yahoo.com or saeed.soliman@alexu.edu.eg
[3] Department of Chemistry, University of Jyväskylä, P.O. Box 35, FI-40014 Jyväskylä, Finland; matti.o.haukka@jyu.fi
[4] Department of Chemistry, College of Science, King Saud University, P.O. Box 2455, Riyadh 11451, Saudi Arabia; amajid@ksu.edu.sa
* Correspondence: ahmed_boraei@science.suez.edu.eg (A.T.A.B.); ambarakat@ksu.edu.sa (A.B.); Tel.: +966-11467-5901 (A.B.); Fax: +966-11467-5992 (A.B.)

Abstract: Four different new Schiff basses tethered indolyl-triazole-3-thione hybrid were designed and synthesized. X-ray single crystal structure, tautomerism, DFT, NBO and Hirshfeld analysis were explored. X-ray crystallographic investigations with the aid of Hirshfeld calculations were used to analyze the molecular packing of the studied systems. The H···H, H···C, S···H, Br···C, O···H, C···C and N···H interactions are the most important in the molecular packing of **3**. In case of **4**, the S···H, N···H, S···C and C···C contacts are the most significant. The results obtained from the DFT calculations indicated that the thione tautomer is energetically lower than the thiol one by 13.9545 and 13.7464 kcal/mol for **3** and **4**, respectively. Hence, the thione tautomer is the most stable one which agree with the reported X-ray structure. In addition, DFT calculations were used to compute the electronic properties while natural bond orbital calculations were used to predict the stabilization energies due to conjugation effects. Both compounds are polar where **4** (3.348 Debye) has a higher dipole moment than **3** (2.430 Debye).

Keywords: Schiff bases; indolyl-triazole-3-thione; tautomerism aspect; Hirshfeld Surface Analysis

Citation: Boraei, A.T.A.; Soliman, S.M.; Haukka, M.; El Tamany, E.S.H.; Al-Majid, A.M.; Barakat, A. X-ray Single Crystal Structure, Tautomerism Aspect, DFT, NBO, and Hirshfeld Surface Analysis of a New Schiff Bases Based on 4-Amino-5-Indol-2-yl-1,2,4-Triazole-3-Thione Hybrid. *Crystals* **2021**, *11*, 1041. https://doi.org/10.3390/cryst11091041

Academic Editors: Assem Barakat, Alexander S. Novikov and Ana M. Garcia-Deibe

Received: 8 August 2021
Accepted: 24 August 2021
Published: 29 August 2021

1. Introduction

Schiff bases are the compounds carrying imine or azomethine (–C=N–) functional groups. These compounds were reported and synthesized for the first time by Hugo Schiff via condensation of carbonyl compounds with the primary amines [1]. Schiff bases are important pharmacological pharmacophores distributed in variety of organic compounds and have many applications in different fields such as inorganic chemistry, biological and analytical chemistry. In the field of pharmaceutical and medicinal chemistry, these compounds also, possess a variety of pharmacological activities including anti-cancer [2], anti-tubercular [3], analgesic [4,5], anti-oxidant [6], anti-inflammatory [7], anthelmintic [8], anti-microbial [9], and so forth.

Indole-triazole-3-thione heterocyclic systems have gained a lot of attention in the research community due to their significant applications in different fields like pharmaceutical, agrochemical, coordination chemistry and biosensor applications [10,11]. Among the biological applications, these indole-triazole-3-thione hybrids have been shown to have strong inhibition activities against many enzymes such as AChE [12], TNF-α [13], (ADAMTS-5) [14], dizinc metallo-β-lactamase [15], and ureases inhibition [16]. Many

synthesized substituted indole-triazole-3-thione systems showed high efficacy and potent pharmacological activities like anti-microbial [17], anti-malarial [18], anti-viral [19], anti-convulsant [20], and anti-proliferative agents [21]. The design and synthesis of new Schiff bases based on the indole-triazole-3-thione hybrid is still of high interest. In planning a development program towards synthesis, a new heterocyclic system is created based on Schiff bases for drug discovery development or material sciences applications.

Our research group has been engaged in a research program about design, synthesis, and spectrophotometric investigations of a variety of heterocyclic systems have been recently reported [22–27]. In this context, we reported the synthesis of four different Schiff bases with the core structure of the indolyl-triazole-3-thione hybrid. The structure of the studied systems was confirmed using a set of spectrophotometric tools and the 3D structure of molecules **3** and **4** is further elucidated unambiguously by single crystal X-ray diffraction technique. Thione-thiol tautomerism was investigated using DFT calculations. In addition, Natural Bond Orbitals (NBO) and Hirshfeld surface analyses of the most stable tautomer were also discussed.

2. Materials and Methods

General

"Melting points were measured using a melting-point apparatus (SMP10) in open capillaries and are uncorrected. The progress of the reaction was observed by thin layer chromatography (TLC) and detection was achieved by UV light. Nuclear magnetic resonance (^{1}H- and ^{13}C-NMR) spectra were determined in DMSO-d_6 and were recorded on a Bruker AC 400 MHz spectrometer using tetramethylsilane as an internal standard. Chemical shifts are described in δ (ppm) and coupling constants are given in Hz. Elemental analysis was performed on a Flash EA-1112 instrument".

2.1. Synthesis

A mixture of 4-amino-5-(1*H*-indol-2-yl)-2,4-dihydro-3*H*-1,2,4-triazole-3-thione **1** (2.0 mmol) and selected benzaldehyde derivatives **2a**–**d** (2.2 mmol) were refluxed in glacial acetic acid (5.0 mL) for 3 h, then cooled. Crystals either developed during cooling the acetic acid solution as in **3**, or crudes of **4**–**6** were filtered, dried and recrystallized from MeOH/DCM mixture. Only, suitable crystals for single crystal X-ray structure measurements were obtained from compounds **3** and **4**.

(E)-4-((4-Bromobenzylidene)amino)-5-(1H-indol-2-yl)-2,4-dihydro-3H-1,2,4-triazole-3-thione (**3**). Yield: 74%, m.p. 231–232 °C [Lit.[28] 222–223 °C]. ^{1}H NMR (400 MHz, DMSO-d_6) δ 14.36 (s, 1 H), 11.94 (s, 1 H), 9.80 (s, 1 H), 7.98 (d, J = 8.5 Hz, 2 H), 7.82 (d, J = 8.5 Hz, 2 H), 7.63 (d, J = 8.0 Hz, 1 H), 7.63 (d, J = 8.0 Hz, 1 H), 7.23–7.20 (m, 1 H), 7.71 (d, J = 1.2 Hz, 1 H), 7.07–7.03 (m, 1 H): ^{13}C NMR (101 MHz, DMSO-d_6) δ 166.10, 162.55, 143.99, 137.48, 132.92, 131.64, 131.13, 127.81, 127.22, 124.27, 122.80, 121.78, 120.43, 112.44, 105.98; elemental analysis calculation for $C_{17}H_{12}BrN_5S$: C, 51.27; H, 3.04; Br, 20.06; N, 17.58; S, 8.05 found: C, 51.46; H, 3.09; Br, 20.01; N, 17.68; S, 8.10.

(E)-4-((2,4-Dichlorobenzylidene)amino)-5-(1H-indol-2-yl)-2,4-dihydro-3H-1,2,4-triazole-3-thione (**4**). Yield: 83%, m.p. 241–242 °C. ^{1}H NMR (400 MHz, DMSO-d_6) δ 14.41 (s, 1 H), 11.92 (s, 1 H), 10.53 (s, 1 H), 8.31 (d, J = 8.5 Hz, 1 H), 7.86 (d, J = 1.9 Hz, 1 H), 7.67 (m, 2 H), 7.48 (d, J = 8.2 Hz, 1 H), 7.27–7.15 (m, 2 H), 7.06 (m, 1H); ^{13}C NMR (101 MHz, DMSO-d_6) δ 162.41, 159.65, 144.31, 138.53, 137.47, 136.65, 130.41, 129.58, 129.25, 129.07, 127.82, 124.25, 122.70, 121.81, 120.40, 112.45, 106.27; elemental analysis calculation for $C_{17}H_{11}C_{l2}N_5S$: C, 52.59; H, 2.86; Cl, 18.26; N, 18.04; S, 8.26 found C, 52.66; H, 2.96; Cl, 18.24; N, 18.12; S, 8.21.

(E)-5-(1H-Indol-2-yl)-4-((2-nitrobenzylidene)amino)-2,4-dihydro-3H-1,2,4-triazole-3-thione (**5**). Yield: 73%, m.p. 243–244 °C. 1H NMR (DMSO-d_6, 400 MHz) δ 14.38 (br.s, 1 H), 11.90 (br.s, 1 H), 10.55 (s, 1 H), 8.30 (d, J = 7.5 Hz, 1 H), 8.24 (d, J = 7.8 Hz, 1 H), 7.88–8.012 (m, 2 H), 7.61 (d, J = 7.8 Hz, 1 H), 7.45 (d, J = 8.4 Hz, 1 H), 7.21 (dd, J = 7.2, 8.4 Hz, 1 H), 7.10 (d, J = 0.9 Hz, 1 H), 7.03 (dd, J = 7.8, 7.2 Hz, 1 H); ^{13}C NMR (101 MHz, DMSO-d_6) δ 162.56, 161.25, 149.32,

144.25, 137.48, 134.85, 133.75, 129.82, 127.79, 126.99, 125.53, 124.30, 122.58, 121.81, 120.42, 112.44, 106.20; elemental analysis calculation for $C_{17}H_{12}N_6O_2S$: C, 56.04; H, 3.32; N, 23.06; S, 8.80 found C, 56.21; H, 3.39; N, 23.01; S, 8.71.

(E)-5-(1H-Indol-2-yl)-4-(((perfluorophenyl)methylene)amino)-2,4-dihydro-3H-1,2,4-triazole-3-thione (**6**). Yield: 88%, m.p. 277–278 °C. ^{1}H NMR (400 MHz, DMSO-d_6) δ 14.46 (s, 1 H), 11.90 (s, 1 H), 10.52 (s, 1 H), 7.63 (d, J = 8.0 Hz, 1 H), 7.46 (d, J = 8.1 Hz, 1 H), 7.26–7.21 (m, 2 H), 7.08–7.05 (m, 1 H); ^{13}C NMR (101 MHz, DMSO-d_6) δ 162.25, 153.55, 144.16, 137.48, 127.95, 127.77, 124.37, 122.54, 121.73, 120.48, 112.42, 106.05; elemental analysis calculation for $C_{17}H_8F_5N_5S$: C, 49.88; H, 1.97; F, 23.21; N, 17.11; S, 7.83 found C, 49.98; H, 2.00; F, 23.22; N, 17.08; S, 7.90.

2.2. Crystal Structure Determination

The experimental results, data collection for the studied compounds, and software used [28–32] were amended in Supplementary Materials.

2.3. Hirshfeld Surface Analysis

The topology analyses were performed using Crystal Explorer 17.5 program [33].

2.4. Computational Methods

"All DFT calculations were performed using Gaussian 09 software package [34,35] with theB3LYP/6-31G(d,p) method. Natural bond orbital analyses were performed using NBO 3.1 program as implemented in the Gaussian 09W package [36]. The self-consistent reaction field (SCRF) method [37,38] was used to model the solvent effects when calculated the optimized geometries in solution".

3. Results and Discussion

3.1. Synthesis of Schiff Bases Based Indolyl-Triazole-3-Thione Hybrid **3**–**6**

The desired Schiff bases **3**–**6** incorporating indolyl-triazole-3-thione hybrid were synthesized according to Scheme 1. In one step condensation reaction of the following substituted aromatic benzaldehydes (**2a**: 4-bromobenzaldehyde; **2b**: 2,4-dichlorobenzaldehyde; **2c**: 2-nitrobenzaldehyde; and **2d**: pentafluorobenzaldehyde) reacted separately with 4-amino-5-(1*H*-indol-2-yl)-2,4-dihydro-3*H*-1,2,4-triazole-3-thione **1** in AcOH under reflux condition for 3 h to afford the target Schiff bases in very good yields. The NMR spectra of the Schiff bases **3**–**6** showed the triazole NH around 14.40 ppm, the indole NH was found at 11.90 ppm, whereas the benzylidene CH=N was detected around 10.50 ppm. The thiocarbonyl group (C=S) was found near 162.50 ppm. Interestingly, compounds **3** and **4** were obtained as crystalline materials subjected to single crystal X-ray diffraction analysis.

3.2. Crystal Structure Description

The X-ray structures of **3** and **4** were determined at 120(2) K. Processing parameters and crystal data are listed in Table 1. Both structures agreed very well with the spectral analyses.

Compound **3** crystallized in the triclinic system and $P\bar{1}$ space group with unit cell parameters of a = 5.9989(2) Å, b = 12.1234(5) Å, c = 13.6872(7) Å, α= 74.972(4)°, β=81.734(4)° and γ = 83.213(3)°. The unit cell volume is 947.98(7) Å^3 and the number of molecules per unit cell is 2, and one molecule per asymmetric unit. Selected bond distances and angles are listed in Table 2. The asymmetric unit comprised one molecule of compound **3** and one acetic acid molecule (Figure 1A). In this compound, the indole and the triazole rings are almost coplanar. The tilt angle between the planes passing through these moieties is found to be 1.64(12)°. In contrast, the 4-bromo-phenyl moiety and the triazole rings are significantly twisted from one another by 59.51(14)°.

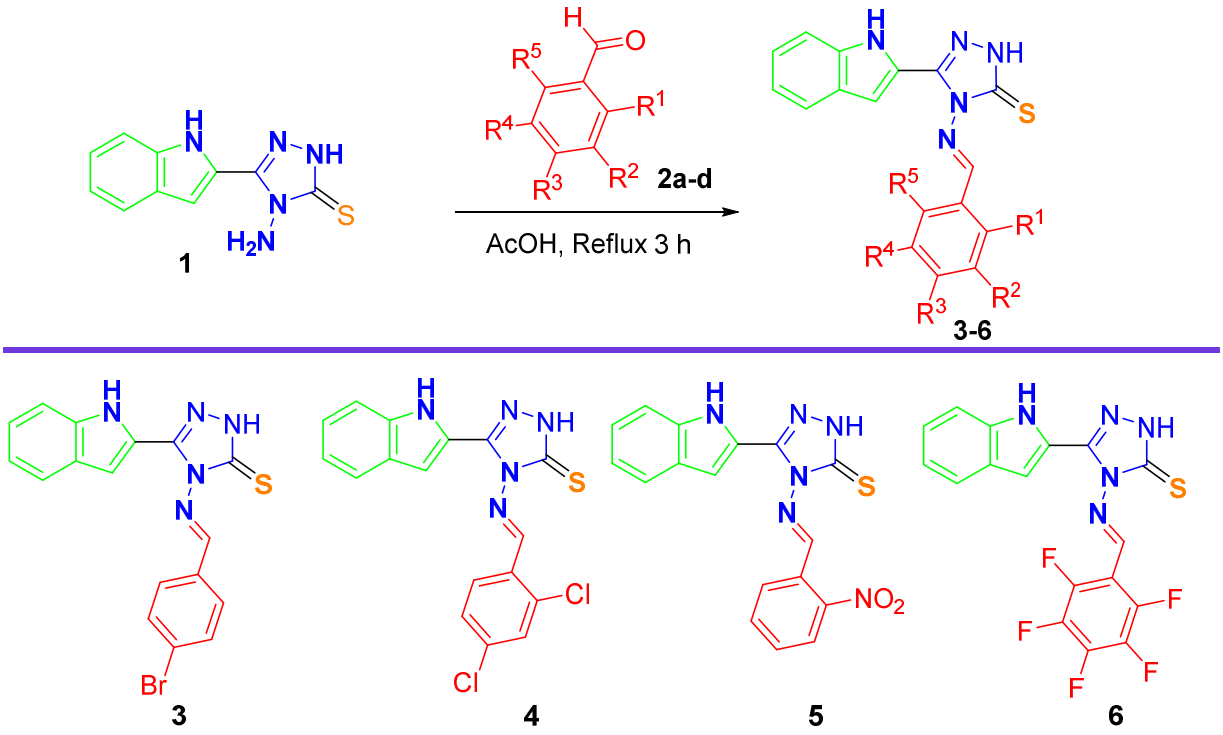

Scheme 1. Synthesis of Schiff bases based indole-triazole-3-thione hybrid **3**–**6**.

Table 1. Crystal Data.

	3	4
CCDC No.	2101946	2101947
Empirical formula	$C_{19}H_{16}BrN_5O_2S$	$C_{17}H_{11}Cl_2N_5S$
Formula weight (g/mol)	458.34	388.27
Temp (K)	120(2)	120(2)
Radiationλ(Å)	1.54184	1.54184
Crystal system	Triclinic	Tetragonal
Space group	$P\bar{1}$	$I4_1/a$
a (Å)	5.9989(2)	32.0004(4)
b (Å)	12.1234(5)	32.0004(4)
c (Å)	13.6872(7)	6.65620(10)
α(deg)	74.972(4)	90
β (deg)	81.734(4)	90
γ(deg)	83.213(3)	90
V (Å^3)	947.98(7)	6816.1(2)
Z	2	16
ρ_{calc} (Mg/m^3)	1.606	1.513
μ (mm^{-1})	4.211	4.660
No. reflns.	9793	16833
Unique reflns.	3541	3538
Completeness to θ = 67.684	100%	99.9%
GOOF (F^2)	1.050	1.031
R_{int}	0.0332	0.0285
R1 [a] ($I \geq 2\sigma$)	0.0591	0.0315
wR2 [b] ($I \geq 2\sigma$)	0.1603	0.0818

[a] $R1 = \Sigma||F_o| - |F_c||/\Sigma|F_o|$. [b] $wR2 = [\Sigma[w(F_o^2 - F_c^2)^2]/\Sigma[w(F_o^2)^2]]^{1/2}$.

Table 2. Selected bond lengths [Å] and angles [°] for **3** and **4**.

Atoms	Distance	Atoms	Distance	Atoms	Distance	Atoms	Distance
	3				**4**		
Br1–C3	1.905(4)	N3-N4	1.376(4)	Cl1-C1	1.7363(15)	N3–C8	1.339(2)
S1–C8	1.685(4)	N4–C9	1.298(5)	Cl2–C3	1.7350(16)	N3–N4	1.3743(18)
N1–C7	1.275(6)	N5–C17	1.367(5)	S1–C8	1.6757(16)	N3–H3	0.88(2)
N1–N2	1.387(5)	N5–C10	1.375(5)	N1–C7	1.264(2)	N4–C9	1.308(2)
N2–C8	1.386(5)	O1–C19	1.312(6)	N1–N2	1.3867(18)	N5–C17	1.371(2)
N2–C9	1.388(5)	O2–C19	1.220(6)	N2–C9	1.3838(19)	N5–C10	1.384(2)
N3–C8	1.332(5)			N2–C8	1.3883(19)		
Atoms	**Angle**	**Atoms**	**Angle**	**Atoms**	**Angle**	**Atoms**	**Angle**
C7–N1–N2	115.3(3)	C5–C6–C1	119.4(4)	C7–N1–N2	118.44(13)	C2–C1–C6	122.12(14)
C8–N2–N1	127.9(3)	C5–C6–C7	119.9(4)	C9–N2–N1	120.03(12)	C2–C1–Cl1	117.36(12)
C8–N2–C9	108.1(3)	C1–C6–C7	120.7(4)	C9–N2–C8	108.05(12)	C6–C1–Cl1	120.51(12)
N1–N2–C9	123.4(3)	N1–C7–C6	119.3(4)	N1–N2–C8	131.87(13)	C1–C2–C3	117.97(14)
C8–N3–N4	114.3(3)			C8–N3–N4	113.99(13)		

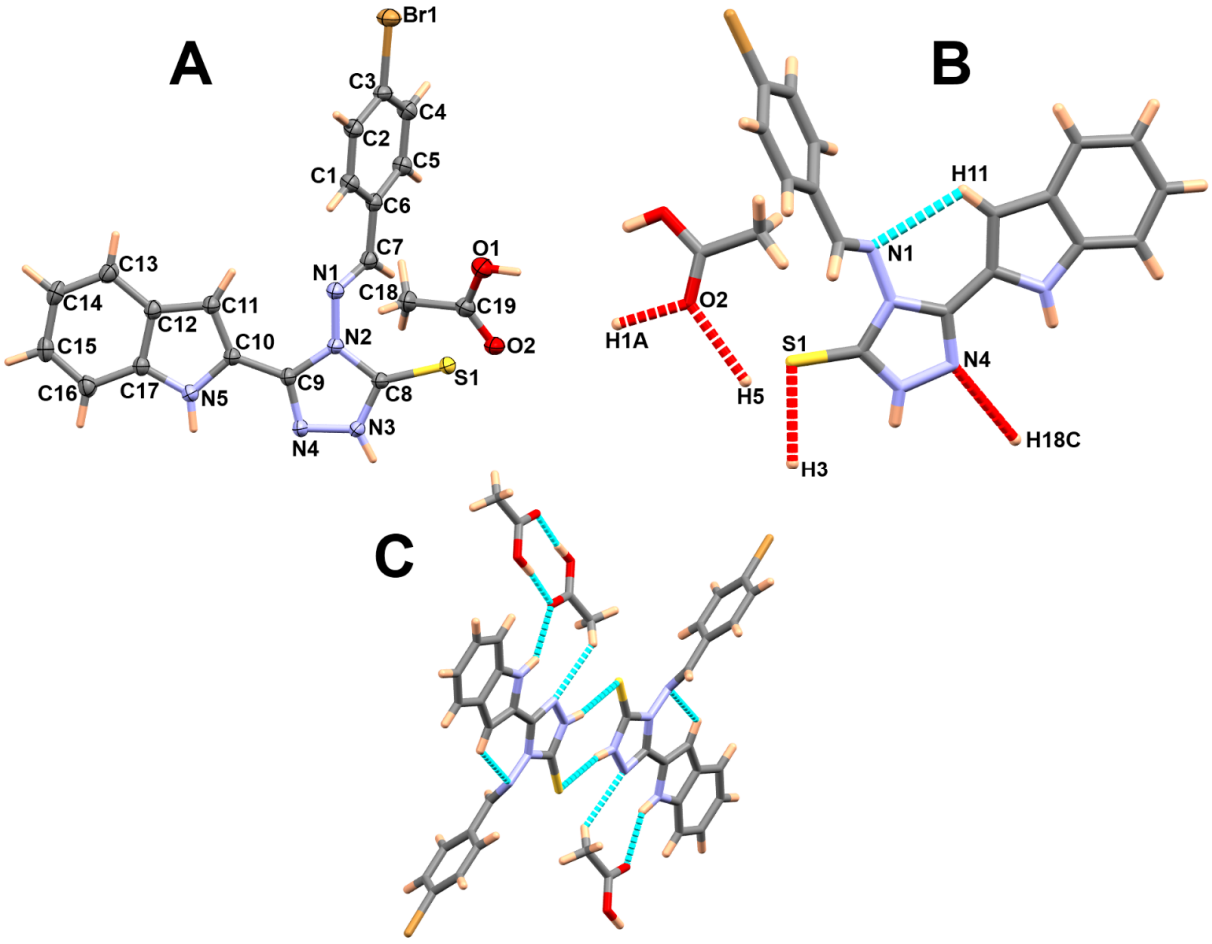

Figure 1. Structure of the asymmetric unit with atomic numbering and thermal ellipsoids drawn at 30% probability (**A**), most important hydrogen bond contacts (**B**) and hydrogen bonding interactions (**C**) in **3**.

The structure of this compound is stabilized by the intramolecular C11–H11···N1 hydrogen bond where the donor-acceptor distance is 3.045(5) Å and hydrogen-acceptor distance of 2.56 Å (Table 3). On the other hand, the molecular units of **3** are packed in the crystal via intermolecular H···S, H···O, and H···N hydrogen bond contacts (Figure 1B). The hydrogen bond parameters of the N3-H3···S1, N5-H5···O2, O1-H1A···O2 and C18-H18C···N4 hydrogen bonding interactions are summarized in Table 3 while presentation of the molecular units held together by these hydrogen bonding contacts is shown in Figure 1C.

Table 3. Hydrogen bonds for **3** and **4** [Å and °].

D–H···A	d(D–H)	d(H···A)	d(D···A)	<(DHA)
		3		
N3–H3···S1$^{\#1}$	0.83	2.43	3.247(3)	170
N5–H5···O2$^{\#2}$	0.86	2.27	3.054(5)	152
C11–H11···N1	0.95	2.56	3.045(5)	112
O1–H1A···O2$^{\#3}$	0.89	1.77	2.662(5)	174
C18–H18C···N4$^{\#2}$	0.98	2.60	3.317(6)	131
$^{\#1}-x, -y, -z+1$; $^{\#2}-x+1, -y, -z+1$; $^{\#3}-x+1, -y, -z$				
		4		
C7–H7···S1	0.95	2.38	3.1578(16)	139
C16–H16···Cl2$^{\#1}$	0.95	2.88	3.3819(17)	114
N5–H5···S1$^{\#2}$	0.86(2)	2.52(2)	3.3293(15)	156(2)
N3–H3···N4$^{\#3}$	0.88(2)	2.11(2)	2.9751(19)	166(2)
$^{\#1}-y+3/4, x+1/4, z-7/4$; $^{\#2}y+1/4, -x+3/4, -z-1/4$; $^{\#3}-y+3/4, x-1/4, -z-1/4$				

The compound **4** crystallized in the more symmetric tetragonal system and the $I4_1/a$ space group. The unit cell parameters are $a = b = 32.0004(4)$ Å, $c = 6.65620(10)$ Å with unit cell volume of 6816.1(2) Å^3 and Z = 16. There is one molecular formula per asymmetric unit (Figure 2A). In this case, the indole and the triazole rings are more twisted from one another by 14.34(13)° compared to that in **3** (1.64(12)°). In addition, the aryl moiety was found less twisted (5.69(11)°) relative to the triazole moiety compared to that in **3** (59.51(14)°). Presentation for the different twists among the connected rings is shown in Figure 3.

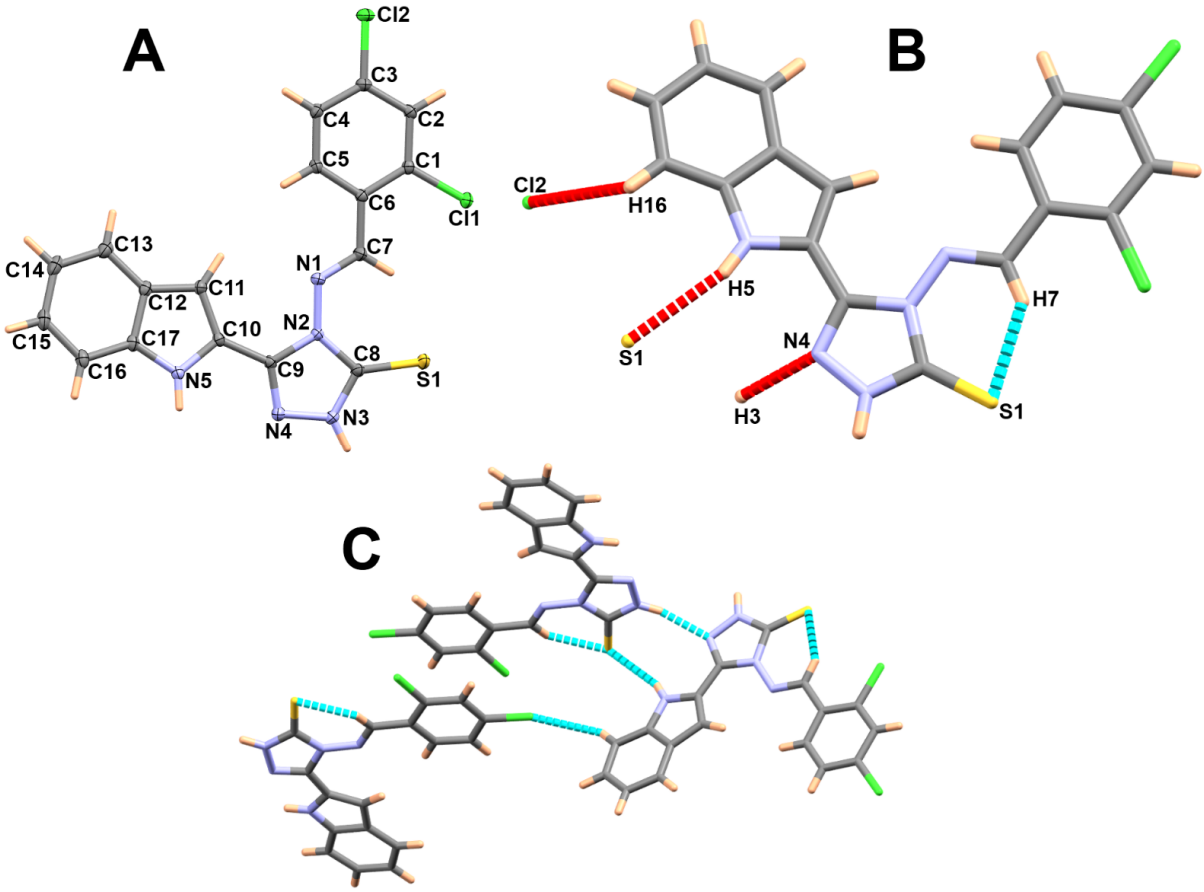

Figure 2. Structure of the asymmetric unit with atomic numbering and thermal ellipsoids drawn at 30% probability (**A**), most important hydrogen bond contacts (**B**) and hydrogen bonding interactions (**C**) in **4**.

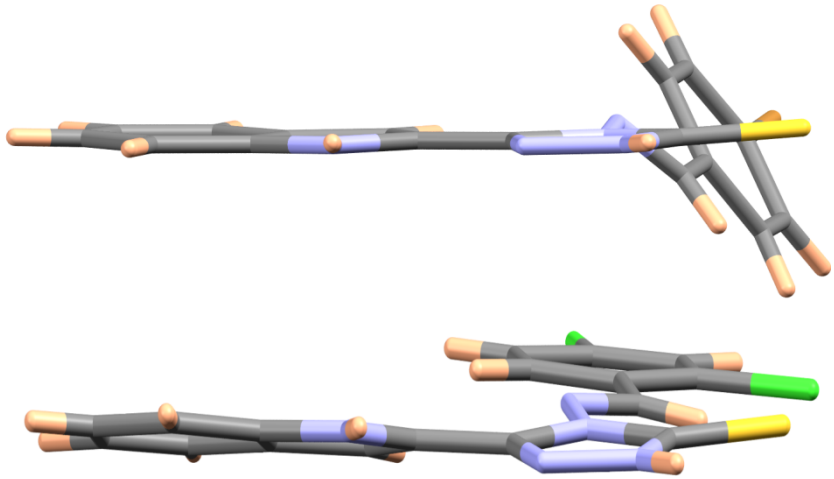

Figure 3. The capped stick model showing the different twists among the three connected ring systems (indole, triazole and aryl moieties) in **3** (higher) and **4** (lower).

Similar to **3**, the molecular structure of compound **4** is stabilized by intramolecular C7–H7···S1 interaction with hydrogen-acceptor and donor-acceptor distances of 2.38 and 3.1578(16) Å, respectively (Table 3). Other intermolecular hydrogen bond contacts affecting the molecular packing are shown in Figure 2B while the molecular packing via these hydrogen bonding interactions is shown in Figure 2C.

3.3. Analysis of Molecular Packing

The Hirshfeld surfaces of **3** are shown in Figure 4. Many red spots were recognized in the d_{norm} map. These regions represent the atomic site included in short intermolecular interactions.

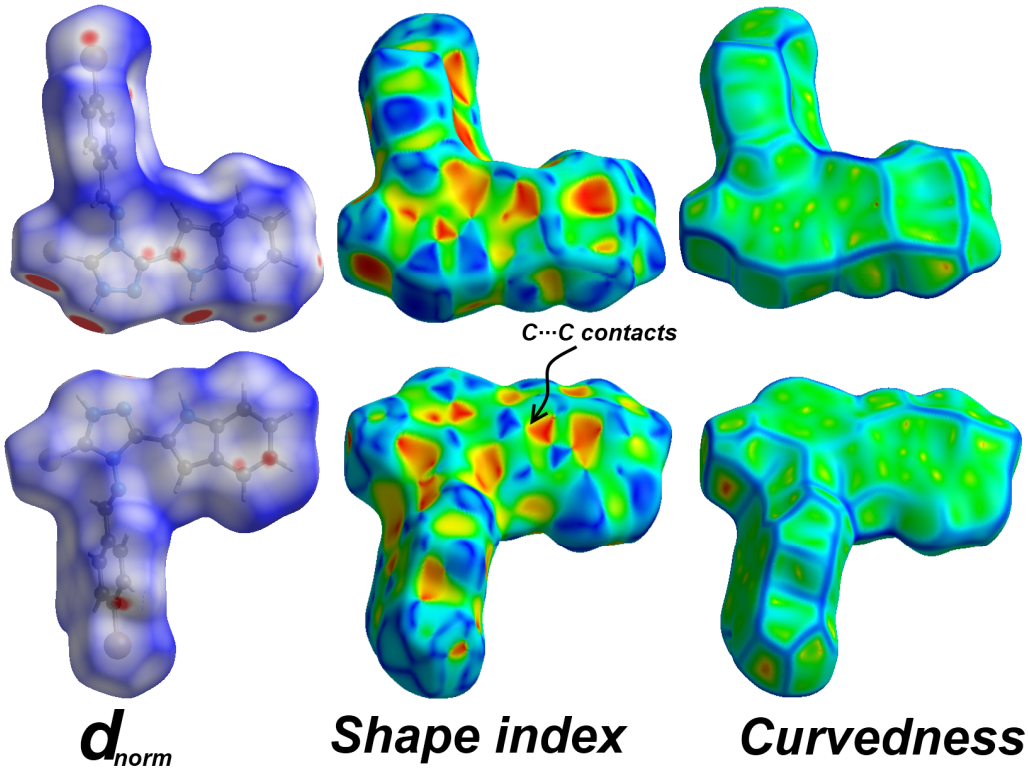

Figure 4. Hirshfeld surfaces of **3**.

Decomposition of the fingerprint plot gave the percentages of all intermolecular contacts in the crystal. The percentages of all possible intermolecular interactions and the decomposed fingerprint plots of the short contacts are presented in Figure 5. It is clear that the H···H (31.8%), H···C (22.4%), S···H (9.8%) and Br···H (8.9%) contacts are the most dominant. In addition, there are some significant contributions from the N···H (5.5%), C···N (5.4%), C···C (5.2%) and O···H (4.4%) contacts.

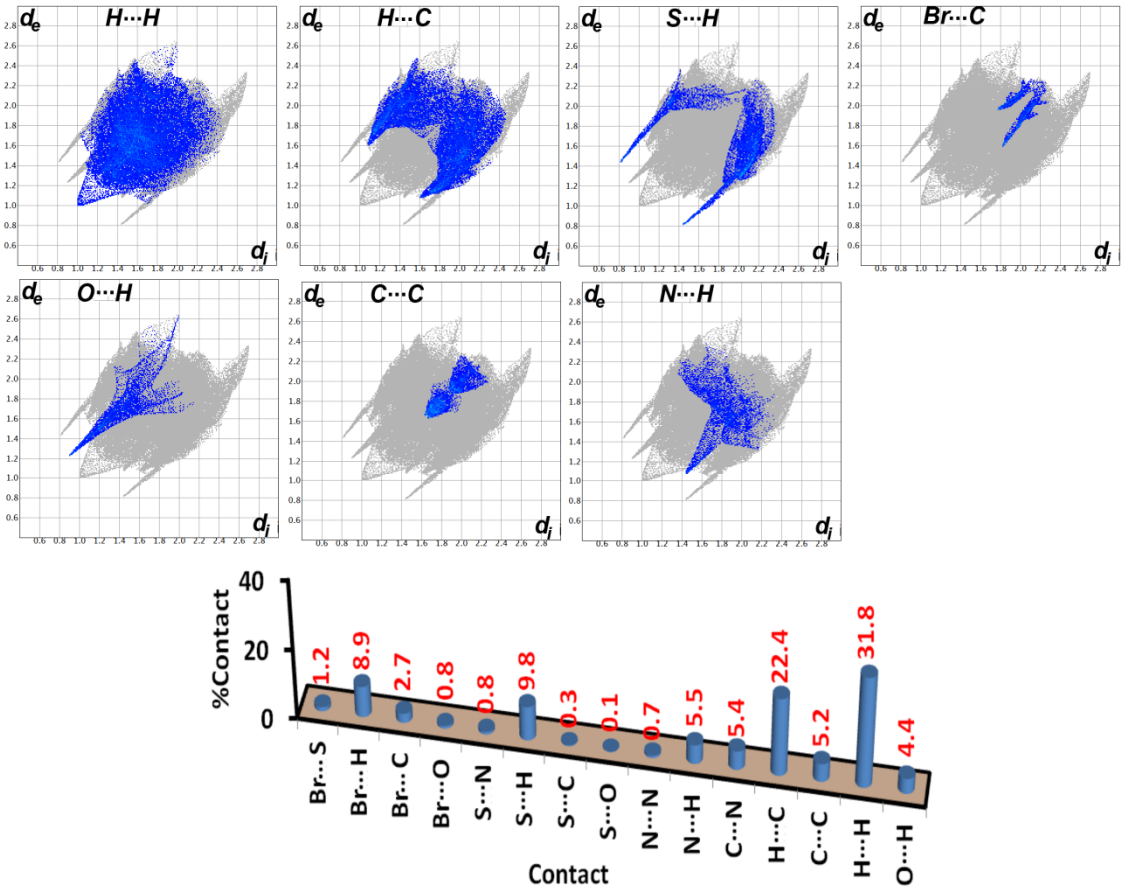

Figure 5. Decomposed fingerprint plots of the most dominant contacts and the percentages of all possible intermolecular interactions in the crystal structure of **3**.

In order to decide which intermolecular contacts are the most significant, the d_{norm} map was decomposed and the results are shown in Figure 6. In this figure, only the contacts appeared as red spots are presented. The results indicated that, the H···H, H···C, S···H, Br···C, O···H, C···C and N···H interactions are the most important as these contacts having shorter distances than the van der Waals radii sum of the interacting atoms. List of the short interaction distances are given in Table 4. The shortest contacts are Br1···C19 (3.421 Å), S1···H3 (2.252 Å), C14···C10 (3.297 Å), H15···C3 (2.693 Å), N4···H18C (2.529 Å), H2···H2 (2.070 Å) and O2···H5 (2.140 Å).

Both of the H···C and S···H contacts appeared as two spikes in the fingerprint plot indicating that the molecule inside the surface acting as hydrogen bond donor and acceptor. In contrast, the O···H and N···H appeared as sharp spikes at the lower left and lower right of the corresponding fingerprint plots, respectively. As a result, the molecule inside the surface acting as hydrogen bond acceptor with respect to the O···H contacts and the hydrogen bond donor is the crystallized acetic acid molecule. The opposite is true for the N···H contacts.

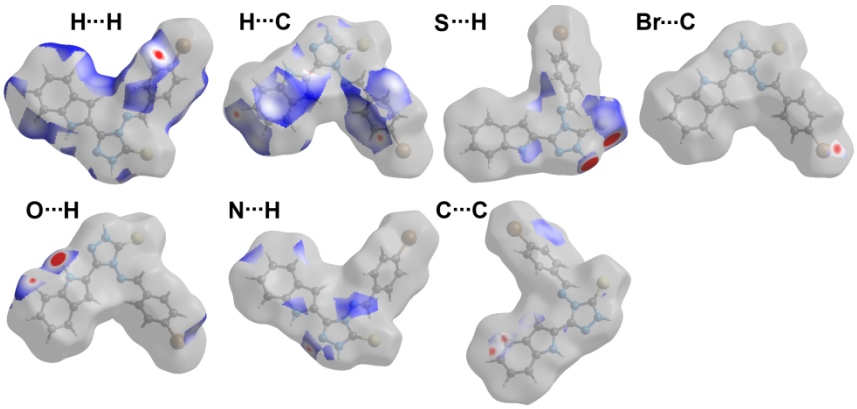

Figure 6. Decomposed d_{norm} maps of the most important contacts in **3**.

Table 4. Most important contacts and the corresponding shortest interaction distances.

Contact	Distance (Å)	Contact	Distance (Å)
Br1···C19	3.421	H15···C3	2.693
S1···H3	2.252	N4···H18C	2.529
C14···C10	3.297	H2···H2	2.070
C8···C11	3.388	O2···H5	2.140
C13···C9	3.324	O1···H16	2.491

Also, the presence of some short C···C contacts (5.2%) related to the aromatic π-system revealed the presence of π–π stacking interactions. This fact was further confirmed by the presence of large green flat area in the curvedness and the complementary red/blue triangles in the shape index (Figure 4).

For compound **4**, the d_{norm}, shape index and curvedness maps are presented in Figure 7. In addition, there are a large number of red spots in d_{norm} map indicating the presence of short contacts which are important for the molecular packing and the crystal stability. These contacts were further analyzed using the fingerprint plot, and their percentages were calculated. The results of decomposed fingerprint plots are depicted in Figure 8. It is obvious that the H···H (26.8%), Cl···H (16.0%), H···C (15.4%), N···H (9.5%), C···C (7.1%) and Cl···C (6.8%) are the most common contacts. The rest of the other interactions and their percentages are presented in the lower part of Figure 8.

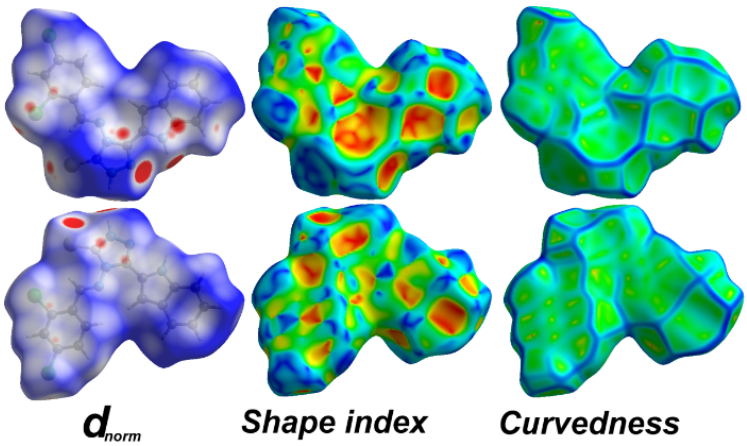

Figure 7. Hirshfeld surfaces of **4**.

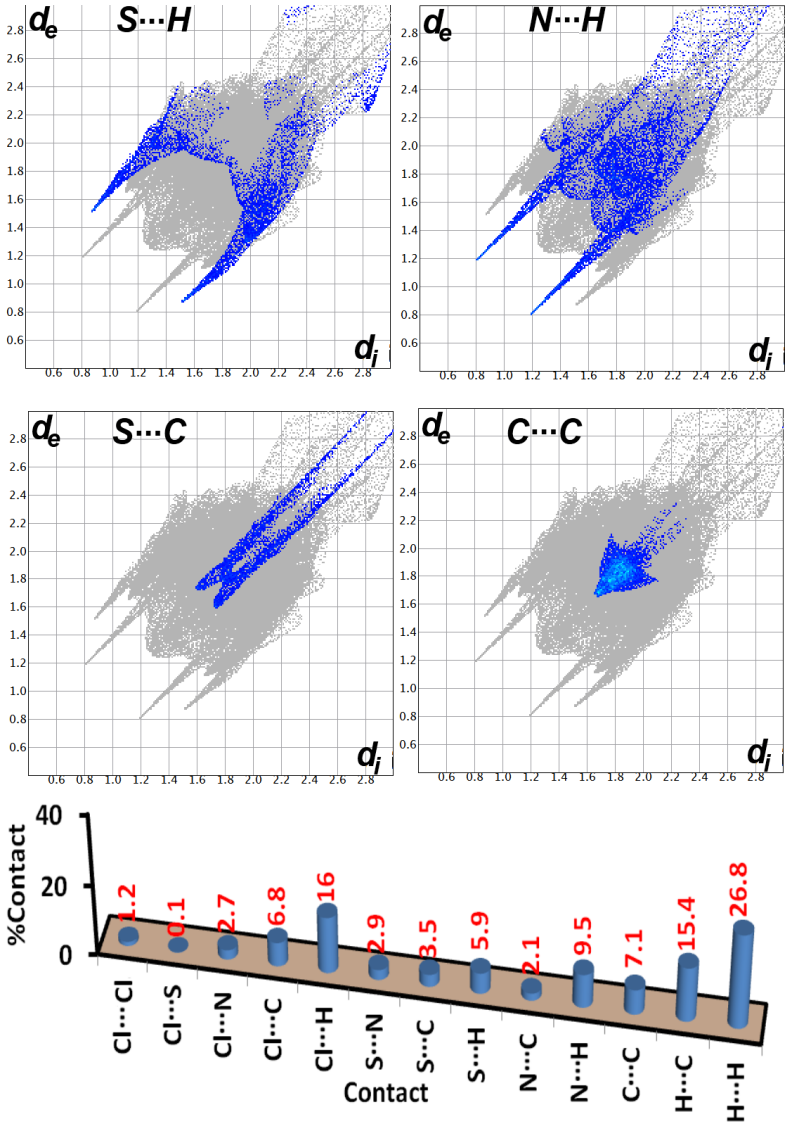

Figure 8. Decomposed fingerprint plots of the most dominant contacts and the percentages of all possible intermolecular interaction in the crystal structure of **4**.

In addition, all S···H and N···H intermolecular contacts appeared in the corresponding decomposed fingerprint plots as two sharp pikes for each interaction. This observation revealed not only the significance of these two contacts in the molecular packing but also shed the light on the contribution of the molecular unit inside the surface in these interactions as hydrogen bond donor and acceptor. As expected, the N···H interactions appeared as sharper spikes indicating shorter interaction distances than the S···H contacts. The importance of these interactions in the molecular packing was also revealed from the appearance of these interactions as intense red regions in the corresponding decomposed d_{norm} maps (Figure 9).

On the other hand, the S···C and C···C contacts appeared as faded red regions in their decomposed d_{norm} maps. In addition, these intermolecular contacts have shorter distances than the vdW radii sum of the interacting atoms. A list of all possible short contacts is given in Table 5. Some other short contacts were also detected such as the Cl1···C17, Cl1···N5, Cl2···H16 and S1···N2 having interactions distances of 3.239, 3.217, 2.829 and 3.304Å, respectively.

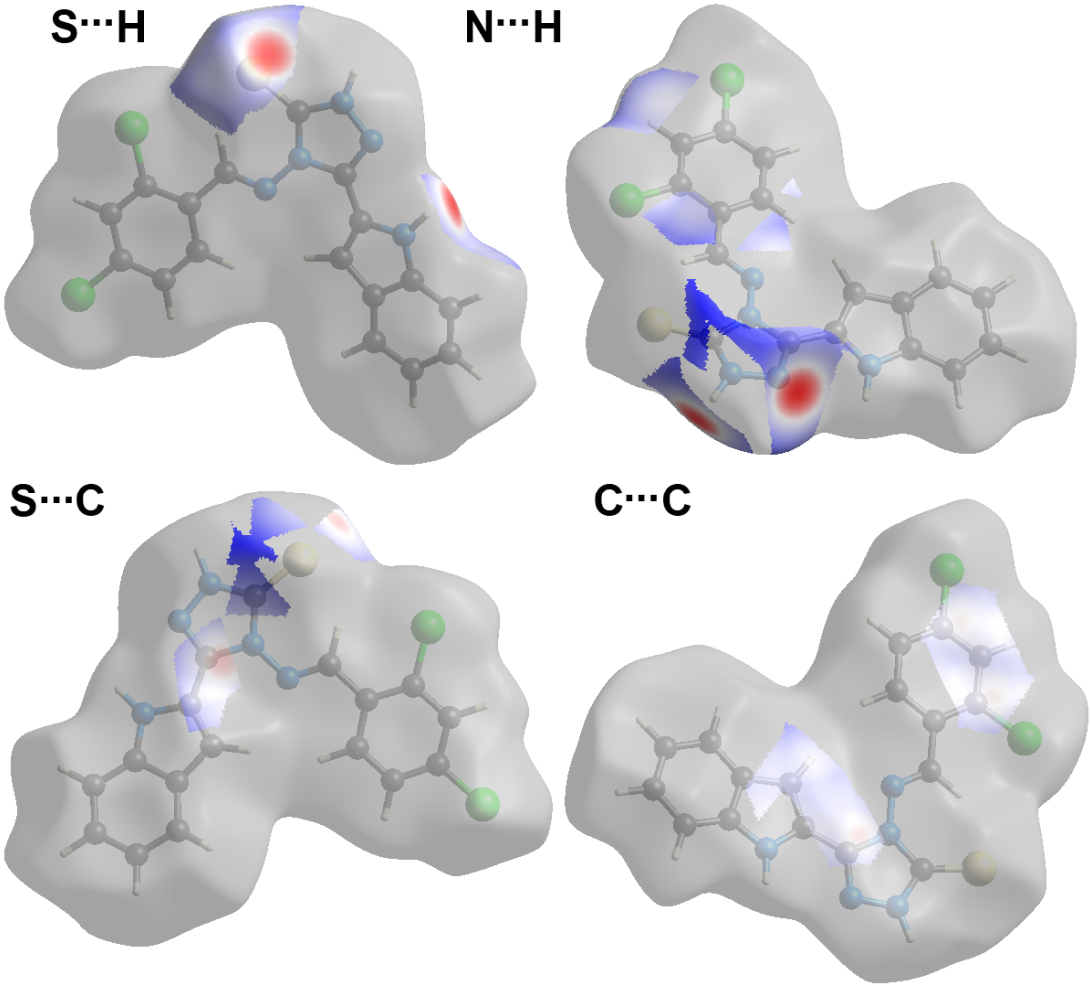

Figure 9. Decomposed d_{norm} maps of the most important contacts in **4**.

Table 5. Most important contacts and the corresponding shortest interaction distances.

Contact	Distance(Å)	Contact	Distance(Å)
Cl1···C17	3.239	S1···N2	3.304
Cl1···N5	3.217	N4···H3	1.99
Cl2···H16	2.829	C9···C1	3.327
S1···H5	2.389	C3···C1	3.356
S1···C9	3.328		

3.4. DFT Studies

3.4.1. Thione-Thiol Tautomerism

The studied compounds could exist in two possible tautomeric forms which are the thione and thiol tautomers. The optimized molecular structures of the thione and thiol tautomers of **3** and **4** are shown in Figure 10. The calculated total energies of both tautomers are listed in Table 6. It is clear that the thione tautomer is energetically lower than the thiol one by 13.9545 and 13.7464 kcal/mol for **3** and **4**, respectively. Hence, the most stable tautomer in gas phase of the studied compounds is the thione form. This conclusion is in good agreement with the reported X-ray structure of the studied compounds. In addition, in solution of the compounds in DMSO, the thione tautomer is energetically lower and could be considered the most stable one. On the other hand, the calculated thermodynamic

parameters indicated that the thione tautomer is the most stable thermodynamically as it has more negative Gibbs free energy compared to the thiol one.

Table 6. Calculated total energies and thermodynamic properties of the thione and thiol tautomers of the studied systems.

		Gas		
	3	**3T1**	**4**	**4T1**
E	−3898.6836	−3898.6572	−2246.7638	−2246.7377
ZPVE [a]	0.2646	0.2605	0.2553	0.2512
E_{corr} [b]	−3898.4190	−3898.3968	−2246.5084	−2246.4865
	−13.9545		−13.7464	
H	−3898.3983	−3898.3757	−2246.4868	−2246.4644
G	−3898.4711	−3898.4492	−2246.5615	−2246.5401
S	153.1780	154.6190	157.2350	159.1760
		DMSO		
	3	**3T1**	**4**	**4T1**
E	−3898.6984	−3898.6723	−2246.7779	−2246.7517
ZPVE [a]	0.2646	0.2602	0.2552	0.2510
E_{corr} [b]	−3898.4338	−3898.4121	−2246.5227	−2246.5007
	−13.5900		−13.8032	
H	−3898.4131	−3898.3909	−2246.5009	−2246.4785
G	−3898.4860	−3898.4650	−2246.5758	−2246.5544
S	153.4790	155.9540	157.6420	159.9290

[a] ZPVE: Zero point vibrational energy correction, [b] E + ZPVE.

3.4.2. Optimized Geometry

The calculated optimized structures of the most stable tautomer of **3** and **4** agreed very well with the reported X-ray structures as indicated from the excellent matching between them (Figure 11). The geometric parameters of the optimized structures are close to the experimental results with some little deviations in the bond distances and bond angles (Table S1 in Supplementary data). In addition, the deviations of the calculated bond distances from the experimental values are very small. For example, the largest deviations occurred for the C22–N5 and C20–N6 in compounds **3** and **4**, respectively. The maximum errors in these cases are 0.027 and 0.019 Å, respectively. The corresponding percentage relative errors are 2.03 and 1.42%, respectively. These deviations could be attributed to the fact that the optimized structures belong to a single molecule in the gas phase which is free from the crystal packing effects. Generally, there are very good straight-line correlations with correlation coefficients (R^2) of 0.994 and 0.968–0.990 for bond distances and angles, respectively (Figure 12).

The studied systems comprised CHNSX (where X=Cl or Br) backbone and differ only in the substituent attached to the phenyl moiety. Graphical presentations of the natural charges at the different atomic sites are shown in Figure 13. The N and S atoms are electronegative where the NH nitrogen is the most electronegative in both compounds. The calculated natural charges at the amine nitrogen are almost the same for both compounds (−0.547 e). The other nitrogen atoms have smaller negative natural charges ranging from −0.225 to −0.303 e and −0.224 to −0.393 e for **3** and **4**, respectively. In addition, the thione S-site has smaller negative natural charges than any of the nitrogen sites which are calculated to be −0.219 and 0.202 e for **3** and **4**, respectively. In contrast, all hydrogen atoms are electropositive where the NH proton has the most positive natural charges. Their natural charge values are calculated to be 0.452 and 0.461 e for **3** and **4**, respectively. On the other hand, the majority of carbon atoms have negative natural charges except those bonded to the N or S atoms where the most positive carbon is the one located between two nitrogen sites in the triazole moiety.

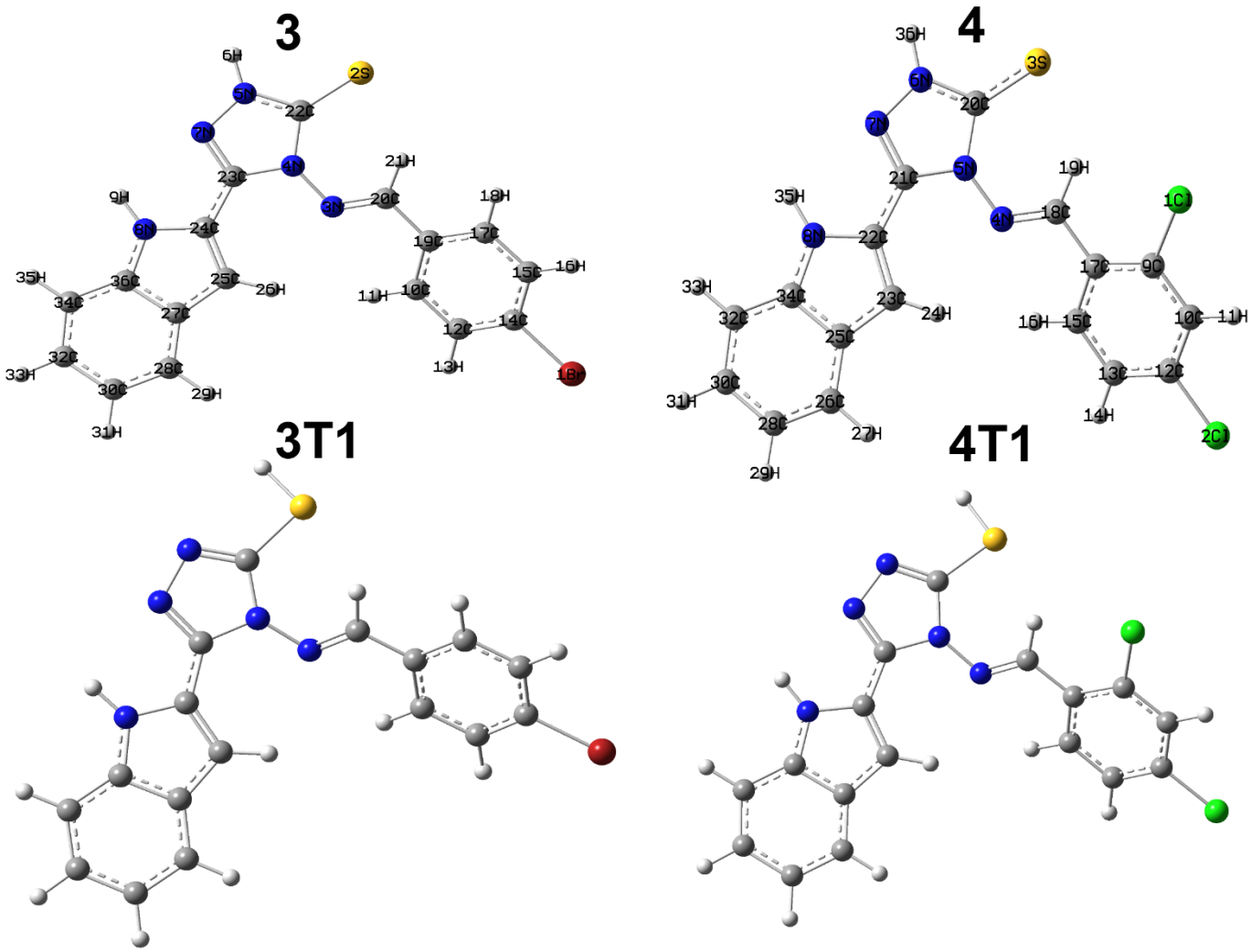

Figure 10. The optimized structures of the thione (**upper**) and thiol (**lower**) tautomers of the studied systems.

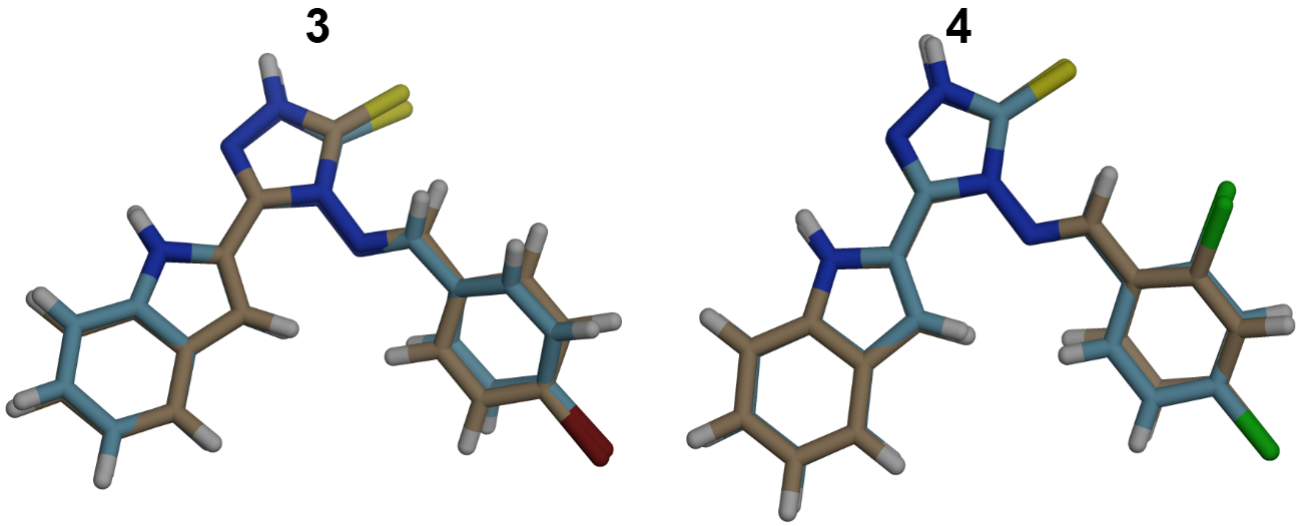

Figure 11. Overlay of the optimized with experimental structures for the studied compounds.

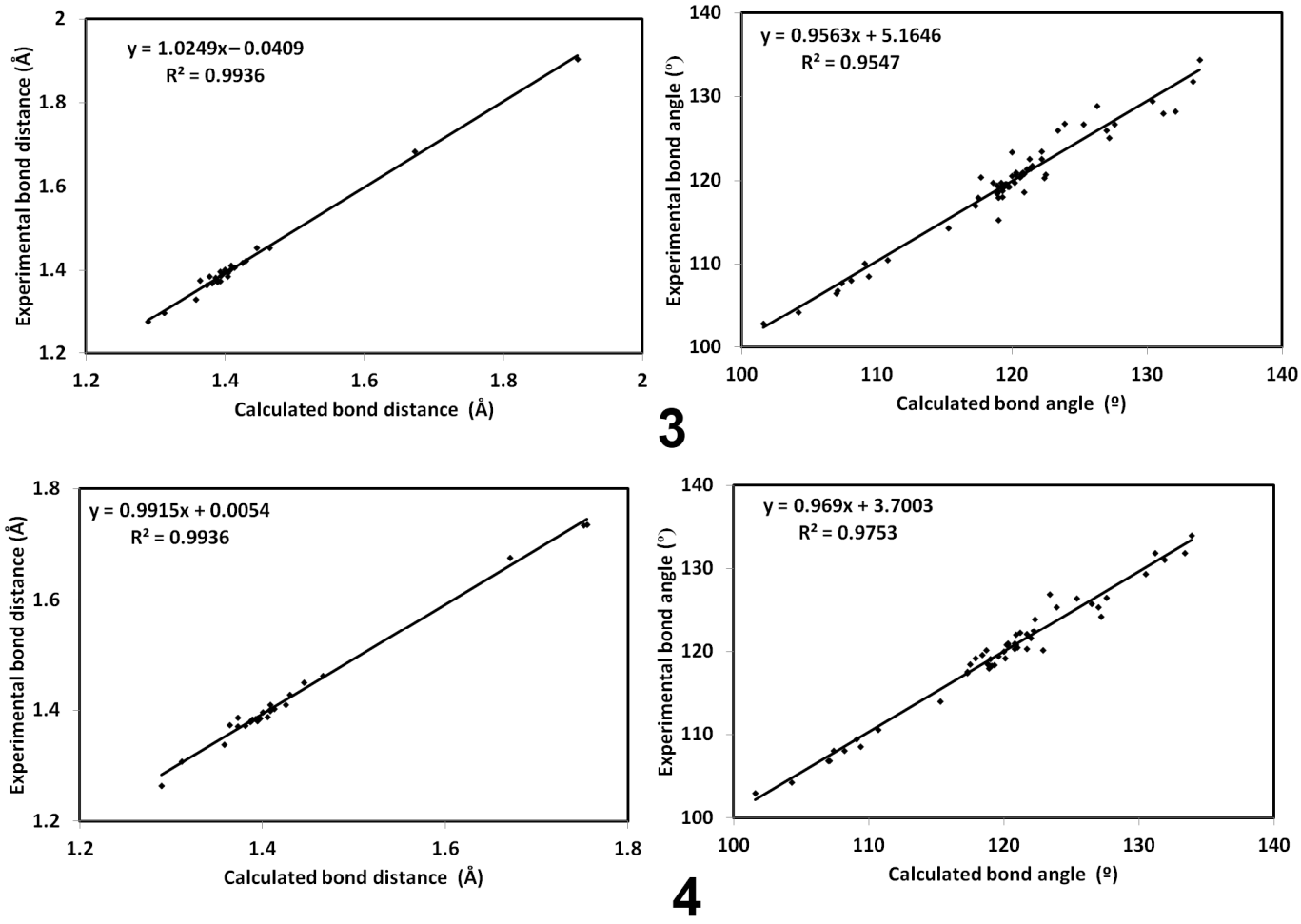

Figure 12. The straight-line correlations between the calculated and experimental geometric parameters.

Both compounds are polar molecules with a net dipole moment of 2.430 and 3.348 Debye for **3** and **4**, respectively. The compound with two chloro substituents at the phenyl ring (**4**) has higher polarity than the one with bromo substituent (**3**). The direction of the dipole moment vector is the same in both compounds as can be seen from Figure 14. In the same figure, the molecular electrostatic potential map (MEP), HOMO and LUMO levels were presented. In MEP map, there are red regions related to the atomic sites with high electron density while the blue regions are related to the atomic sites with the lowest electron density.

On the other hand, the HOMO and LUMO levels have almost similar patterns in both compounds. The HOMO level is located mainly over the delocalized π-system and the thione S-atom while the LUMO level is distributed over the π-system (Figure 14). Hence, the excitation from the HOMO to LUMO level could be described as mixed π–π* and n-π* excitations. The HOMO→LUMO excitation energies are calculated to be 3.466 and 3.462 eV for **3** and **4**, respectively.

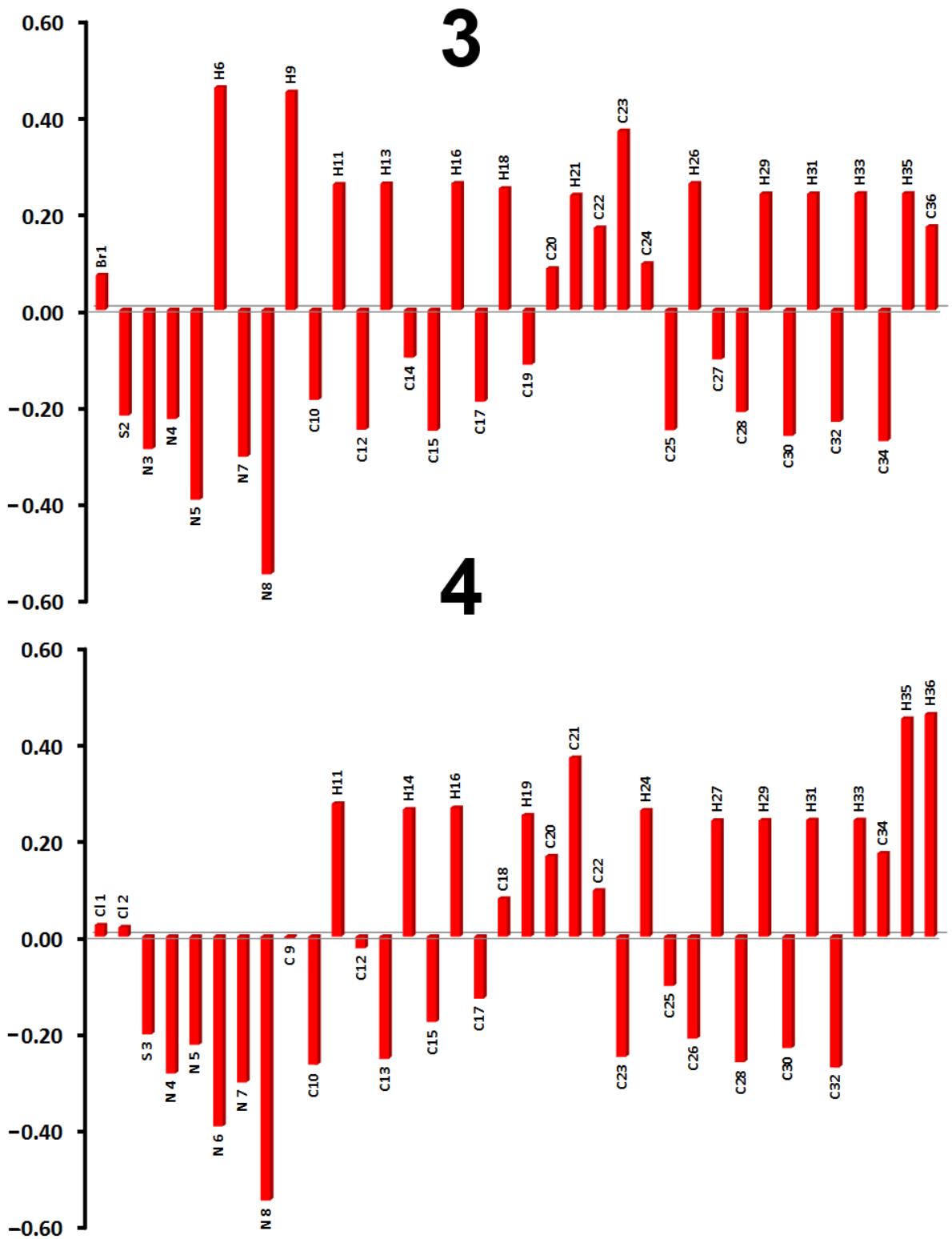

Figure 13. Natural charge population at the different atomic sites for the studied compounds (Table S2; Supplementary data).

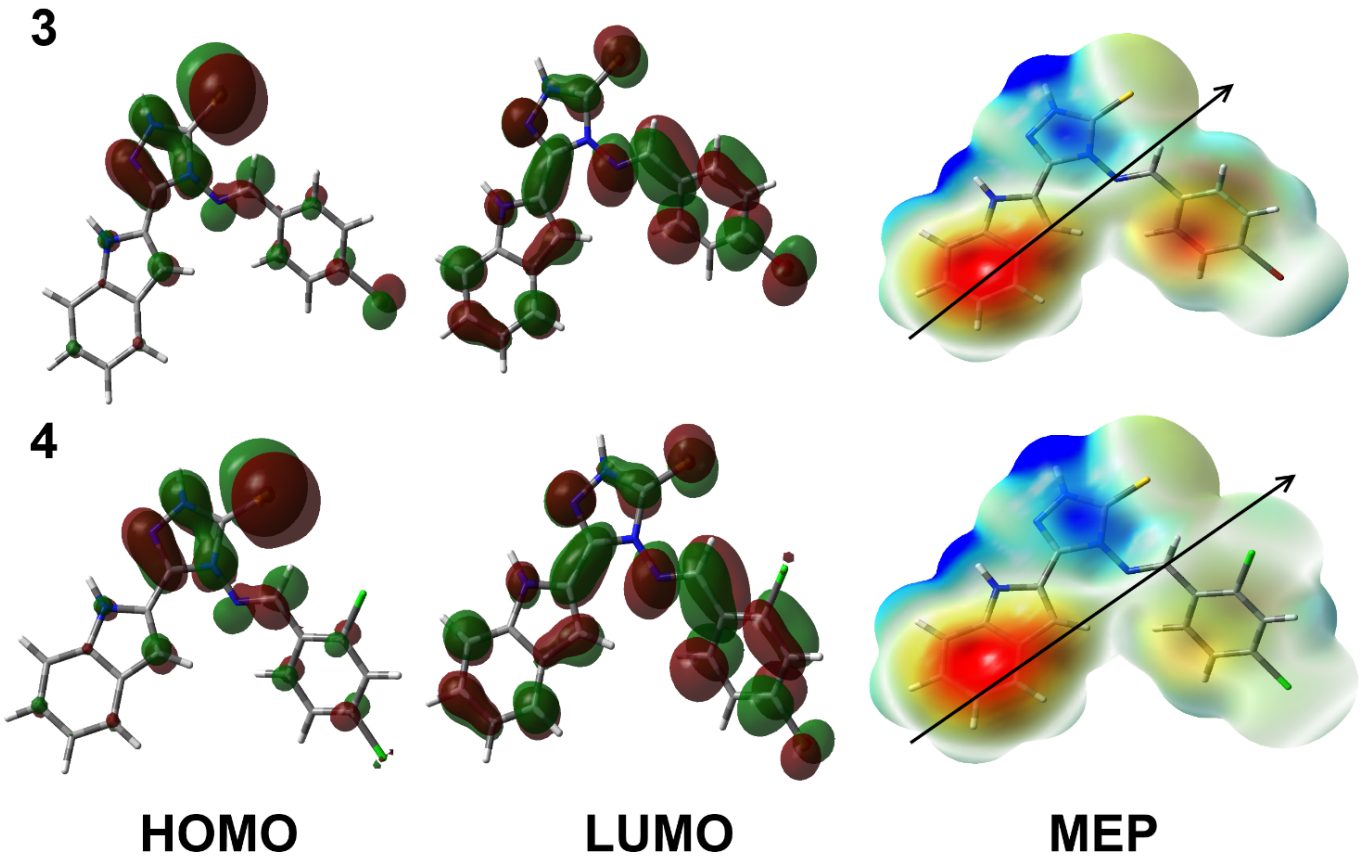

Figure 14. The MEP, HOMO and LUMO for the studied compounds.

3.4.3. Electronic Reactivity Parameters

The HOMO and LUMO energies are important parameters for calculating molecular reactivity parameters such as ionization potential (I= $-E_{HOMO}$), electron affinity (A=$-E_{LUMO}$), chemical potential ($\mu = -(I + A)/2$), hardness ($\eta = (I - A)/2$) as well as electrophilicity index ($\omega = \mu^2/2\eta$). These reactivity indices were calculated [39–44] and listed in Table 7. The ionization potential and electron affinity values of **3** are lower than **4**. Similarly, the electrophilicity index is lower for **3** than **4**. In contrast, the hardness and chemical potential are higher for the former than the latter.

Table 7. Reactivity parameters of the studied compounds.

Parameter	3	4
E_{HOMO}	−5.5904	−5.6320
E_{LUMO}	−2.1241	−2.2858
I	5.5904	5.6320
A	2.1241	2.2858
η	3.4662	3.3462
μ	−3.8572	−3.9589
ω	2.1462	2.3419

3.5. NBO Analysis

The process of conjugation has a great importance in the stability of the molecular system [45,46]. These intramolecular charge transfer (IMCT) and their stabilization energies ($E^{(2)}$) are summarized in Table 8. Compounds **3** and **4** are stabilized σ–σ*, π→π*, n→σ* and n→π* IMCT processes. These processes stabilized the structure of **3** up to 6.99, 22.24, 10.55 and 43.94 kcal/mol, respectively which are corresponding to BD(1)C25–C27→

BD*(1)C23–C24, BD(2)C24–C25→ BD*(2)N7–C23, LP(2)S2→ BD*(1)N5–C22 and LP(1)N4→ BD*(2)N7–C23, respectively. The corresponding values for **4** are 6.99, 22.26, 13.24 and 43.50 kcal/mol for the BD(1)C23–C25→ BD*(1)C21–C22, BD(2)C22–C23→ BD*(2)N7–C21, LP(2)S3→ BD*(1)N5–C20 a BD*(1)N5–C20 and LP(1)N5→ BD*(2)N7–C21, respectively.

Table 8. The $E^{(2)}$ (kcal/mol) values for the IMCTprocesses in **3** and **4** [a].

Donor NBO	Acceptor NBO	$E^{(2)}$(kcal/mol)	Donor NBO	Acceptor NBO	$E^{(2)}$ (kcal/mol)
3			**4**		
σ→σ*					
BD(1)N5–N7	BD*(1)C23–C24	5.92	BD(1)N6–N7	BD*(1)C21–C22	5.92
BD(1)C19–C20	BD*(1)N3–N4	5.46	BD(1)C17–C18	BD*(1)N4–N5	5.46
BD(1)C25–C27	BD*(1)C23–C24	6.99	BD(1)C23–C25	BD*(1)C21–C22	6.99
BD(1)C32–C34	BD*(1)N8–C36	6.20	BD(1)C30–C32	BD*(1)N8–C34	6.20
π→π*					
BD(2)N3–C20	BD*(2)C17–C19	7.7	BD(2)N4–C18	BD*(2)C9–C17	8.33
BD(2)N7–C23	BD*(2)C24–C25	9.26	BD(2)N7–C21	BD*(2)C22–C23	9.27
BD(2)C10–C12	BD*(2)C14–C15	20.99	BD(2)C9–C17	BD*(2)N4–C18	16.54
BD(2)C10–C12	BD*(2)C17–C19	18.5	BD(2)C9–C17	BD*(2)C10–C12	20.13
BD(2)C14–C15	BD*(2)C10–C12	17.71	BD(2)C9–C17	BD*(2)C13–C15	18.34
BD(2)C14–C15	BD*(2)C17–C19	19.41	BD(2)C10–C12	BD*(2)C9–C17	19.44
BD(2)C17–C19	BD*(2)N3–C20	20.6	BD(2)C10–C12	BD*(2)C13–C15	17.02
BD(2)C17–C19	BD*(2)C10–C12	19.53	BD(2)C13–C15	BD*(2)C9–C17	18.97
BD(2)C17–C19	BD*(2)C14–C15	21.31	BD(2)C13–C15	BD*(2)C10–C12	21.72
BD(2)C24–C25	BD*(2)N7–C23	22.24	BD(2)C22–C23	BD*(2)N7–C21	22.26
BD(2)C24–C25	BD*(2)C27–C36	15.59	BD(2)C22–C23	BD*(2)C25–C34	15.57
BD(2)C27–C36	BD*(2)C24–C25	19.79	BD(2)C25–C34	BD*(2)C26–C28	18.92
BD(2)C27–C36	BD*(2)C28–C30	18.95	BD(2)C25–C34	BD*(2)C30–C32	17.36
BD(2)C27–C36	BD*(2)C32–C34	17.4	BD(2)C26–C28	BD*(2)C25–C34	16.39
BD(2)C28–C30	BD*(2)C27–C36	16.37	BD(2)C26–C28	BD*(2)C30–C32	19.64
BD(2)C28–C30	BD*(2)C32–C34	19.65	BD(2)C30–C32	BD*(2)C25–C34	19.69
BD(2)C32–C34	BD*(2)C27–C36	19.67	BD(2)C30–C32	BD*(2)C26–C28	16.65
BD(2)C32–C34	BD*(2)C28–C30	16.64			
n→σ*					
LP(2)S2	BD*(1)N4–C22	13.1	LP(2)S3	BD*(1)N5–C20	13.24
LP(2)S2	BD*(1)N5–C22	10.55	LP(2)S3	BD*(1)N6–C20	10.72
LP(1)N3	BD*(1)N4–C22	10.38	LP(1)N4	BD*(1)N5–C20	10.56
LP(1)N3	BD*(1)C20–H21	9.14	LP(1)N4	BD*(1)C18–H19	8.84
LP(1)N7	BD*(1)N4–C23	7.54	LP(1)N7	BD*(1)N5–C21	7.57
LP(1)N7	BD*(1)N5–C22	7.75	LP(1)N7	BD*(1)N6–C20	7.75
n→π*					
LP(3)Br1	BD*(2)C14–C15	10.2	LP(3)Cl2	BD*(2)C10–C12	12.94
LP(1)N4	BD*(2)N3–C20	19.62	LP(1)N5	BD*(2)N4–C18	20.68
LP(1)N4	BD*(2)N7–C23	43.94	LP(1)N5	BD*(2)N7–C21	43.50
LP(1)N5	BD*(2)N7–C23	25.96	LP(1)N6	BD*(2)N7–C21	26.00
LP(1)N8	BD*(2)C24–C25	36.66	LP(1)N8	BD*(2)C22–C23	36.73
LP(1)N8	BD*(2)C27–C36	37.44	LP(1)N8	BD*(2)C25–C34	37.44

[a] Atom numbering refer to Figure 10.

4. Conclusions

Four substituted (*E*)-4-(benzylidene)amino)-5-(1*H*-indol-2-yl)-1,2,4-triazole-3-thione Schiff bases **3**–**6** were synthesized and characterized. One step condensation reaction furnished the requisite compounds in high chemical yield. Two single crystals were obtained **3**–**4**. The thione-thiol tautomerism in the studied compounds was investigated using DFT calculations. The results indicated that the thione tautomer is more stable than the thiol one for both compounds. The supramolecular structures of **3** and **4** were analyzed using Hirshfeld calculations. The H···H, H···C, S···H, Br···C, O···H, C···C and N···H in **3** and the S···H, N···H, S···C and C···C contacts in **4** are the most important in the molecular packing and crystal stability. Different IMCT interactions which stabilize their molecular

structures were predicted with the aid of NBO calculations. Further investigation towards application of the synthesized Schiff bases based indolyl-triazole-3-thione hybrid will be considered in the near future.

Supplementary Materials: The following are available online at https://www.mdpi.com/article/10.3390/cryst11091041/s1, X-ray structure determinations; Figures S1–S8: ^{1}H NMR and ^{13}C NMR of the Schiff bases **3**–**6**, Tables S1 and S2: The calculated geometric parameters and natural charges of **3** and **4**.

Author Contributions: Conceptualization, A.T.A.B., S.M.S. and A.B.; synthesis and characterization, A.T.A.B., E.S.H.E.T. and A.M.A.-M.; X-ray crystal structure carried out by: M.H.; computational investigation done by: S.M.S., writing original manuscript, A.T.A.B., S.M.S. and A.B.; revision and editing, A.T.A.B., S.M.S. and A.B. All authors have read and agreed to the published version of the manuscript.

Funding: Researchers Supporting Project (RSP-2021/64), King Saud University, Riyadh, Saudi Arabia.

Data Availability Statement: Not Applicable.

Acknowledgments: The authors would like to extend their sincere appreciation to the Researchers Supporting Project (RSP-2021/64), King Saud University, Riyadh, Saudi Arabia.

Conflicts of Interest: The authors declare no conflict of interest.

References

1. Schiff, H. Mittheilungen aus dem Universitatslaboratorium in Pisa: Eine neue reihe organischer Basen. *Justus Liebigs Ann. Chem.* **1864**, *131*, 118–119. [CrossRef]
2. Ali, S.M.M.; Azad, M.A.K.; Jesmin, M.; Ahsan, S.; Rahman, M.M.; Khanam, J.A.; Islam, M.N.; Shahriar, S.M.S. In vivo anticancer activity of vanillin semicarbazone. *Asian Pac. J.Trop. Biomed.* **2012**, *2*, 438–442. [CrossRef]
3. Aboul-Fadl, T.; Mohammed, F.A.H.; Hassan, E.A.S. Synthesis, antitubercular activity and pharmacokinetic studies of some Schiff bases derived from 1-alkylisatin and isonicotinic acid hydrazide (INH). *Arch. Pharm. Res.* **2003**, *26*, 778–784. [CrossRef]
4. Chandramouli, C.; Shivanand, M.R.; Nayanbhai, T.B.; Bheemachari, B.; Udupi, R.H. Synthesis and biological screening of certain new triazole Schiff bases and their derivatives bearing substituted benzothiazole moiety. *J. Chem. Pharm. Res.* **2012**, *4*, 1151–1159.
5. Sondhi, S.M.; Singh, N.; Kumar, A.; Lozach, O.; Meijer, L. Synthesis, anti-inflammatory, analgesic and kinase (CDK-1, CDK-5 and GSK-3) inhibition activity evaluation of benzimidazole/benzoxazole derivatives and some Schiff's bases. *Bioorg. Med. Chem.* **2006**, *14*, 3758–3765. [CrossRef] [PubMed]
6. Wei, D.; Li, N.; Lu, G.; Yao, K. Synthesis, catalytic and biological activity of novel dinuclear copper complex with Schiff base. *Sci. China Ser. B Chem.* **2006**, *49*, 225–229. [CrossRef]
7. Sathe, B.S.; Jaychandran, E.; Jagtap, V.A.; Sreenivasa, G.M. Synthesis characterization and anti-inflammatory evaluation of new fluorobenzothiazole schiff's bases. *Int. J. Pharm. Res. Dev.* **2011**, *3*, 164–169.
8. Avaji, P.G.; Kumar, C.V.; Patil, S.A.; Shivananda, K.N.; Nagaraju, C. Synthesis, spectral characterization, in-vitro microbiological evaluation and cytotoxic activities of novel macrocyclic bis hydrazone. *Eur. J. Med. Chem.* **2009**, *44*, 3552–3559. [CrossRef] [PubMed]
9. Gomha, S.M.; Riyadh, S.M. Synthesis under microwave irradiation of [1,2,4]triazolo[3,4-*b*][1,3,4]thiadiazoles and other diazoles bearing indole moieties and their antimicrobial evaluation. *Molecules* **2011**, *16*, 8244–8256. [CrossRef]
10. Darestani-Farahani, M.; Faridbod, F.; Ganjali, M.R. A sensitive fluorometric DNA nano biosensor based on a new fluorophore for tumor suppressor gene detection. *Talanta* **2018**, *190*, 140–146. [CrossRef] [PubMed]
11. Chhrouri, M.; Othman, A.A.; Jiménez-Cecilia, S.; Moreno-Cabrerizo, C.; Sansano, J.M. 4-Amino-3-pentadecyl-3*H*-1,2,4-triazole-3-thions and 3-pentadecyl-1,3,4-oxadiazole-2(3*H*)-thione for the preparation of dimeric palladium (II) complexes and their applications in Tsuji–Trostand Mizoroki–Heck reactions. *Synth. Commun.* **2019**, *49*, 1301–1307. [CrossRef]
12. Timur, İ.; Kocyigit, Ü.M.; Dastan, T.; Sandal, S.; Ceribası, A.O.; Taslimi, P.; Gulcin, İ.; Koparir, M.; Karatepe, M.; Çiftçi, M. In vitro cytotoxic and invivo antitumoral activities of some aminomethylderivatives of 2,4-dihydro-3*H*-1,2,4-triazole-3-thiones—Evaluation of their acetylcholinesterase and carbonicanhydrase enzymes inhibitionprofiles. *J. Biochem. Mol. Toxic.* **2019**, *33*, e22239. [CrossRef] [PubMed]
13. Gilmore, J.L.; King, B.W.; Asakawa, N.; Harrison, K.; Tebben, A.; Sheppeck, J.E., II; Liu, R.Q.; Covington, M.; Duan, J.J.W. Synthesis and structure–activity relationship of anovel, non-hydroxamate series of TNF-α converting enzyme inhibitors. *Bioorg. Med. Chem. Lett.* **2007**, *17*, 4678–4682. [CrossRef] [PubMed]
14. Maingot, L.; Leroux, F.; Landry, V.; Dumont, J.; Nagase, H.; Villoutreix, B.; Sperandio, O.; Deprez-Poulain, R.; Deprez, B. Newnon-hydroxamic ADAMTS-5 inhibitors based on the 1,2,4-triazole-3-thiols caffold. *Bioorg. Med. Chem. Lett.* **2010**, *20*, 6213–6216. [CrossRef]

15. Sevaille, L.; Gavara, L.; Bebrone, C.; DeLuca, F.; Nauton, L.; Achard, M.; Mercuri, P.; Tanfoni, S.; Borgianni, L.; Guyon, C.; et al. 1,2,4-Triazole-3-thione compounds as inhibitors of dizincmetallo-β-lactamases. *ChemMedChem* **2017**, *12*, 972–985. [CrossRef] [PubMed]
16. Akhtar, T.; Hameed, S.; Khan, K.M.; Choudhary, M.I. Syntheses,urease inhibition, and antimicrobial studies of some chiral 3-substituted-4-amino-5-thioxo-1*H*,4*H*-1,2,4-triazoles. *Med. Chem.* **2008**, *4*, 539–543. [CrossRef]
17. Chen, M.; Lu, S.; Yuan, G.; Yang, S.; Du, X. Synthesis and antibacterial activity of some heterocyclic β-enamino ester derivatives with 1,2,3-triazole. *Heterocycl. Commun.* **2000**, *6*, 421–426. [CrossRef]
18. Gujjar, R.; Marwaha, A.; El Mazouni, F.; White, J.; White, K.L.; Creason, S.; Shackleford, D.M.; Baldwin, J.; Charman, W.N.; Buckner, F.S.; et al. Identification of ametabolically stable triazolopyrimidine-based dihydroorotatede hydrogenase inhibitor with antimalarial activity in mice. *J. Med. Chem.* **2009**, *52*, 1864–1872. [CrossRef]
19. Huang, M.; Deng, Z.; Tian, J.; Liu, T. Synthesis and biological evaluation of salinomycintriazole analogues as anticancer agents. *Eur. J. Med. Chem.* **2017**, *127*, 900–908. [CrossRef]
20. Ayati, A.; Emami, S.; Foroumadi, A. The importance of triazole scaffold in the development of anticonvulsant agents. *Eur. J. Med. Chem.* **2016**, *109*, 380–392. [CrossRef]
21. Mohammad, Y.; Fazili, K.M.; Bhat, K.A.; Ara, T. Synthesis and biological evaluation of novel 3-*O*-tethered triazoles of diosgenin as potent antiproliferative agents. *Steroids* **2017**, *118*, 1–8.
22. Boraei, A.T.; Singh, P.K.; Sechi, M.; Satta, S. Discovery of novel functionalized 1, 2, 4-triazoles as PARP-1 inhibitors in breast cancer: Design, synthesis and antitumor activity evaluation. *Eur. J. Med. Chem.* **2019**, *182*, 111621. [CrossRef]
23. Boraei, A.T.; Ashour, H.K.; El Sayed, H.; Abdelmoaty, N.; El-Falouji, A.I.; Gomaa, M.S. Design and synthesis of new phthalazine-based derivatives as potential EGFR inhibitors for the treatment of hepatocellular carcinoma. *Bioorg. Chem.* **2019**, *85*, 293–307. [CrossRef] [PubMed]
24. Boraei, A.T.; Sarhan, A.A.; Yousuf, S.; Barakat, A. Synthesis of a New Series of Nitrogen/Sulfur Heterocycles by Linking Four Rings: Indole; 1, 2, 4-Triazole; Pyridazine; and Quinoxaline. *Molecules* **2020**, *25*, 450. [CrossRef] [PubMed]
25. Boraei, A.T.; Haukka, M.; Soliman, S.M.; Barakat, A. Synthesis, X-ray structure, tautomerism aspect, and chemical insight of the 3-(1*H*-Indol-2-yl)-7*H*-[1, 2, 4] triazolo [3, 4-*b*][1, 3, 4] thiadiazin-6-ol. *J. Mol. Struct.* **2021**, *1227*, 129429. [CrossRef]
26. Boraei, A.T.; Soliman, S.M.; Haukka, M.; Barakat, A. X-Ray structure, Hirshfeld analysis and DFT studies of two new hits of triazolyl-indole bearing alkylsulfanyl moieties. *J. Mol. Struct.* **2021**, *1225*, 129302. [CrossRef]
27. Boraei, A.T.; Soliman, S.M.; Yousuf, S.; Barakat, A. Synthesis single crystal x-ray structure dft studies and hirshfeld analysis of new benzylsulfanyl-triazolyl-indole scaffold. *Crystals* **2020**, *10*, 685. [CrossRef]
28. Rikagu Oxford Diffraction. *CrysAlisPro*; Agilent Technologies Inc.: Yarnton, UK, 2018.
29. Sheldrick, G.M. SHELXT - Integrated space-group and crystal-structure determination. *Acta Cryst.* **2015**, *A71*, 3–8. [CrossRef]
30. Sheldrick, G.M. Crystal structure refinement with *SHELXL*. *Acta Cryst.* **2015**, *C71*, 3–8.
31. Hübschle, C.B.; Sheldrick, G.M.; Dittrich, B.J. ShelXle: A Qt graphical user interface for SHELXL. *J. Appl. Crystallogr.* **2011**, *44*, 1281–1284. [CrossRef]
32. Turner, M.J.; McKinnon, J.J.; Wolff, S.K.; Grimwood, D.J.; Spackman, P.R.; Jayatilaka, D.; Spackman, M.A. Crystal Explorer17. University of Western Australia. 2017. Available online: http://hirshfeldsurface.net (accessed on 12 June 2017).
33. Frisch, M.J.; Trucks, G.W.; Schlegel, H.B.; Scuseria, G.E.; Robb, M.A.; Cheeseman, J.R.; Scalmani, G.; Barone, V.; Mennucci, B.; Petersson, G.A.; et al. *GAUSSIAN 09*; Revision A02; Gaussian Inc.: Wallingford, CT, USA, 2009.
34. Dennington, R., II; Keith, T.; Millam, J. (Eds.) *GaussView*; Version 4.1; Semichem Inc.: Shawnee Mission, KS, USA, 2007.
35. Reed, A.E.; Curtiss, L.A.; Weinhold, F. Intermolecular interactions from a natural bond orbital, donor-acceptor viewpoint. *Chem. Rev.* **1988**, *88*, 899–926. [CrossRef]
36. Cheeseman, J.R.; Trucks, G.W.; Keith, T.A.; Frisch, M.J. A Comparison of Models for Calculating Nuclear Magnetic Resonance Shielding Tensors. *J. Chem. Phys.* **1996**, *104*, 5497–5509. [CrossRef]
37. Marten, B.; Kim, K.; Cortis, C.; Friesner, R.A.; Murphy, R.B.; Ringnalda, M.N.; Sitkoff, D.; Honig, B. New Model for Calculation of Solvation Free Energies: Correction of Self-Consistent Reaction Field Continuum Dielectric Theory for Short-Range Hydrogen-Bonding Effects. *J. Phys. Chem.* **1996**, *100*, 11775–11788. [CrossRef]
38. Tannor, D.J.; Marten, B.; Murphy, R.; Friesner, R.A.; Sitkoff, D.; Nicholls, A.; Ringnalda, M.; Goddard, W.A.; Honig, B. Accurate first principles calculation of molecular charge distributions and solvation energies from ab initio quantum mechanics and continuum dielectric theory. *J. Am. Chem. Soc.* **1994**, *116*, 11875–11882. [CrossRef]
39. Foresman, J.B.; Frisch, E. *Exploring Chemistry with Electronic Structure Methods*, 2nd ed.; Gaussian: Pittsburgh, PA, USA, 1996.
40. Chang, R. *Chemistry*, 7th ed.; McGraw-Hill: New York, NY, USA, 2001.
41. Kosar, B.; Albayrak, C. Spectroscopic investigations and quantum chemical computational study of (E)-4-methoxy-2-[(p-tolylimino) methyl] phenol. *Spectrochim. Acta* **2011**, *78*, 160–167. [CrossRef] [PubMed]
42. Koopmans, T.A. Ordering of wave functions and eigenenergies to the individual electrons of an atom. *Physica* **1933**, *1*, 104–113. [CrossRef]
43. Parr, R.G.; Yang, W. *Density—Functional Theory of Atoms and Molecules*; Oxford University Press: New York, NY, USA, 1989.

44. Parr, R.G.; Szentpaly, L.V.; Liu, S. Electrophilicity index. *J. Am. Chem. Soc.* **1999**, *121*, 1922–1924. [CrossRef]
45. Hubert Joe, I.; Kostova, I.; Ravikumar, C.; Amalanathan, M.; Pinzaru, S.C. Theoretical and vibrational spectral investigation of sodium salt of acenocoumarol. *J. Raman Spectrosc.* **2009**, *40*, 1033–1038.
46. Sebastian, S.; Sundaraganesan, N. The spectroscopic (FT-IR, FT-IR gas phase, FT-Raman and UV) and NBO analysis of 4-Hydroxypiperidine by density functional method. *Spectrochim. Acta Part. A Mol. Biomol. Spectrosc.* **2010**, *75*, 941–952. [CrossRef]